eprints@whiterose.ac.uk
https://eprints.whiterose.ac.uk/

Molecular Survey of Strongly and Weakly Interfacially Active Asphaltenes: An Intermolecular Force Field Approach

Ballard, D.A.[1], Pickering, J.H.[2], Rosbottom, I.[3], Tangparitkul, S.[4], Roberts, K.J.[1], Rae, R.[5], Dowding, P.J.[5], Hammond, R.B.[1] and Harbottle, D.[1*]

1) School of Chemical and Process Engineering, University of Leeds, Leeds, UK.
2) School of Computing, University of Leeds, Leeds, UK.
3) Department of Chemical Engineering, Imperial College London, London, UK.
4) Department of Mining and Petroleum Engineering, Faculty of Engineering, Chiang Mai University, Chiang Mai, 50200, Thailand.
5) Infineum UK Ltd., Abingdon, Oxfordshire, UK.

ABSTRACT

Sub-fractionation of asphaltenes based on their interfacial activity has begun to highlight critical differences between those asphaltenes that are strongly interfacially active (IAA) and the remaining asphaltenes (RA). Following the methods of Petroleomics, representative structures of the two asphaltene fractions were determined, reflecting differences in abundant heteroatom groups, carbon number, double bond equivalents, and single-core/multi-core motifs. Using atomistic-potential based grid-search methods, the intermolecular interactions between asphaltene-asphaltene and asphaltene-solvent (water, heptane and toluene) were rapidly screened to identify the most favorable, and therefore most likely intermolecular interactions to occur. Asphaltene-water interactions were stronger for IAA (abundance-weighted average interaction energy of -9.29 kJ/mol) than RA (-6.32 kJ/mol), with hydrogen bonding more significant in the IAA-H_2O interaction. Dimer interactions of IAA-IAA were stronger than RA-RA, and from the top 100 most favored interactions, the contribution to the total interaction energy was almost exclusively van der Waals for RA-RA (only 3% electrostatic), while for IAA-IAA, electrostatic interactions (9%) and hydrogen bonding (2%) were significant contributors in the most favored interactions. As the relative contribution of the electrostatic interaction increased, the dimer orientation less resembled that of a π-π stack. With the conception of Petroleomics and large structural databases, the grid-search method is a useful atomic/molecular screening approach that provides an ideal triaging tool to rapidly assess a wide range of different molecular structures and interactions. The method is

complementary to the more computationally-expensive precision molecular modelling tools that are not suited to such workflows.

INTRODUCTION

Asphaltenes are the heavy components of crude oil which are typically defined as being soluble in aromatic solvents and insoluble in aliphatic solvents. However, this solubility classification provides little understanding of their physicochemical properties, even though these properties strongly govern their problematic behavior in the crude oil. Developing a clearer understanding of how intermolecular structure and chemistry dictate interactions between different components within asphaltene fractions and consequently their development as nanoaggregates is important as it strongly correlates to their stability in the crude oil. Hence, elucidating and characterizing the prominent interactions has the potential to provide new insights at the functional molecular scale, aiding the design better performing asphaltene dispersants.

Recent research has attempted to summarize and achieve a consensus regarding the physicochemical properties of asphaltenes.[1-3] Despite this, the common understanding of asphaltene structure and their interaction mechanisms remains a matter of current debate and one being refined. Indeed, through advancement of analytical techniques such as FT-ICR MS, a much greater clarity has emerged about the overall chemical architecture of asphaltene molecules. Consequently novel mechanisms describing asphaltenes intermolecular-interactions have been proposed.[4-7] While the Yen-Mullins model is based on the concept of interacting aromatic cores (π-π stacking),[8] contributions from asphaltene chemistry have also been associated with polymer-like and supramolecular-like structures to account for the other interactions associated with heteroatoms content, heteroatoms functional groups and metals content.[9-11] Recently, Zhang et al. proposed a new hypothesis for asphaltenes aggregation involving free radical interactions or pancake bonding,[7] where the authors comment that the persistence of stable free radical PAHs and their interaction with diverse PAHs result in stronger aggregate interactions. Importantly, the authors comment that pancake bonding is complementary to π-π stacking, as well as interactions associated with the heteroatoms.

Methods to fractionate asphaltenes have begun to highlight important differences in asphaltene chemistry associated with changes in the asphaltene aromaticity, size and polarity.[12-19] Some of these early studies fractionated asphaltenes based on their affinity to partition at either an

oil-water or oil-CaCO$_3$ interface, with the subsequent characterization of these fractions providing new insight to relate the asphaltene chemistry to asphaltenes stability and deposition tendency. The methods to separate strongly interfacially active asphaltenes from whole asphaltenes are described in full in Yang et al.[14] and Subramanian et al..[15] Elemental analysis of the IAA fraction confirmed an increase in O and S content and a slight reduction in asphaltene aromaticity. SANS studies also highlighted differences in the asphaltenes nanoaggregate structures, with the behavior attributed to the functional group chemistry of the asphaltene subfractions.[20] Interrogation of the strongly- and weakly-interfacially active asphaltenes by FT-ICR MS has revealed an enrichment of polar, less aromatic multi-core structures, which are strongly-interfacially active, hence presenting an enhanced picture of the physicochemical properties of the asphaltene fraction.[6]

Whilst molecular dynamics (MD) simulations have been used to probe and understand the aggregation mechanisms of asphaltenes, difficulties have often arisen due to their complex chemistry and the computationally intensive requirements when studying such large molecules. Kuznicki et al.[21] used MD to probe the interactions between model asphaltene molecules, based on large continental (island-like) motifs with heteroatoms in the aromatic core and attached aliphatic chains. The heteroatoms in the aliphatic chains which were either associated or disassociated (anionic), with the study revealing the anionic asphaltenes to preferentially interact at the water-toluene interface. The research revealed that the aggregation mechanism was independent of the asphaltene type with aggregation via stacking of the polyaromatic rings. Similar observations were reported by Headen et al.[22] who simulated the formation of dimers and trimers using typical island-like an archipelago-like motifs. These authors also highlighted the reversibility of aggregate formation in toluene, attributing this to its preferred T-stacked or offset-stacked aggregation geometry. For the archipelago-like motif, the authors commented on the difficulty in determining the likely interaction mechanism between two asphaltene molecules due to the limitations of MD in terms of obtaining satisfactory statistics in reasonable timescales. Larger multi-core structures were also considered by Yang et al.,[13] who proposed molecular representations of asphaltenes that are strongly- and weakly-interfacially active. These authors confirmed that there was a difference in interfacial activity of the model asphaltene motifs highlighting that there was a greater affinity for the strongly-interfacially active asphaltenes to self-associate within the bulk solvent. Due to the physicochemical complexity of the model asphaltene structures, the authors limited their analysis to aggregation mechanisms involving π-π stacking and sulfur-sulfur interactions. Although π-π interactions

were found to contribute to the self-association of both asphaltene fractions, the interaction was found to be weaker in the strongly-interfacially active asphaltenes due to a higher steric hindrance. The work highlighted the strong polarity of sulfoxide groups promotes intermolecular hydrogen bonding between the sulfoxide-aromatic core notably between the O heteroatom within the sulfoxide group and hydrogen atoms near to the sulfoxide group in a neighboring molecule.

Overall, the combination of the complex asphaltenes chemistry and the diversity of structural types mean that modeling of the systems using MD becomes computationally expensive, which, in turn, restricts maximum simulation times to be a few hundred nanoseconds,[22-24] which is likely insufficient to determine their steady-state structures.[25-27] Such a computational expense can be reduced through the use of meso-scale (more granular) methods such as dissipative particle dynamics (DPD),[28] which can enable longer times through coarse graining, albeit at the expense of lowering the simulation accuracy. Using molecular grid-search methods offer an attractive and alternative approach in that it systematically surveys the interaction energies on the atomistic scale between interacting molecules and has been used extensively to provide insights into solution chemistry and crystallization by calculating solute/solute, solute/solvent and solvent/solvent interactions.[29-32] Similar interaction energy calculations have been used to predict the aggregation of coronene (polycyclic aromatic hydrocarbon with six rings) and asphaltenes.[33, 34] With computational times less than one minute on a single processor, this approach provides an attractive methodology combining the advantage of rapid screening and atomic specific granularity, which enables calculations of (thermodynamically) energetically stable intermolecular configurations for many molecular structures.[31, 35, 36]

Specifically, the current study utilises a systematic, grid-search method to calculate the interaction energies between the five most abundant asphaltene motifs in each of the two asphaltene fractions, i.e. interfacially active asphaltenes (IAA) and remaining asphaltenes (RA). In this study, the optimal interactions between multiple structures including asphaltene-asphaltene and asphaltene-solvent are examined to provide greater insight into the dominant interactions and structures of nanoaggregates in the whole asphaltene fraction. The main objective is to show the potential of the grid-search method to rapidly screen interactions in complex mixtures. Over the last decade the science of Petroleomics has created opportunity to develop databases of asphaltene structures,[37-39] of which tens-of-thousands of structures have

been reported. With such a large database of structures, typical modelling tools such as MD would not be appropriate to rapidly screen molecule-molecule interactions due to the significant computational time. This is not a limitation of the grid-search method and the current study was used to demonstrate this principal using typical asphaltene molecules that were determined following the methods of Petroleomics.

MATERIALS AND EXPERIMENTAL METHODS

Structure Optimization: Based on previous determinations,[6] the structures of RA and IAA considered here are shown in Fig. 1. These structures were proposed based on the elemental groups of HC, N_xO_y/N_x, O_x, O_xS_y and S_x, with the relative abundance of these groups found to represent 93% of IAA and 91% of RA.

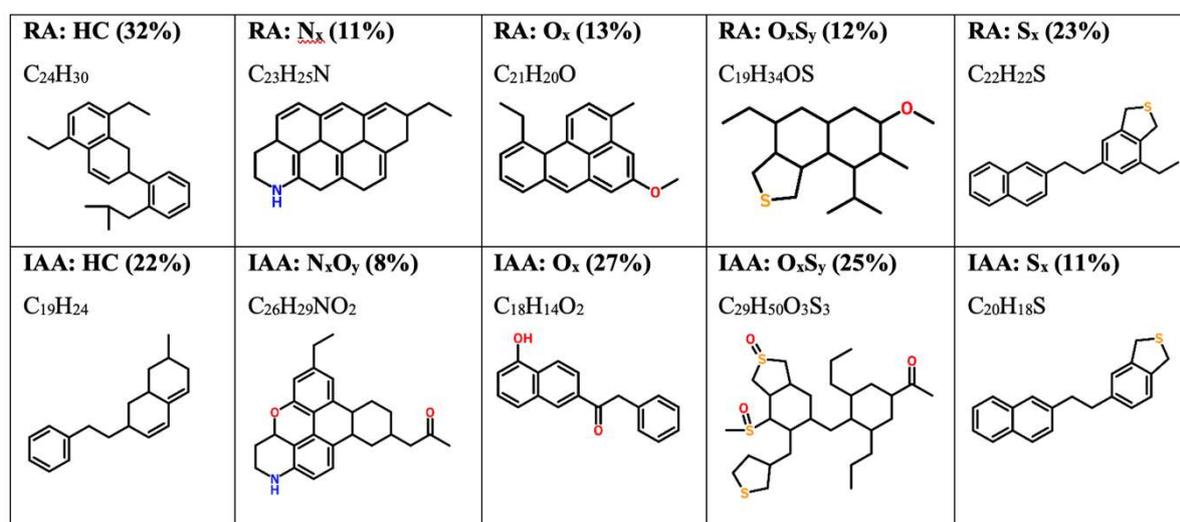| RA: HC (32%)	RA: N_x (11%)	RA: O_x (13%)	RA: O_xS_y (12%)	RA: S_x (23%)
$C_{24}H_{30}$	$C_{23}H_{25}N$	$C_{21}H_{20}O$	$C_{19}H_{34}OS$	$C_{22}H_{22}S$
IAA: HC (22%)	IAA: N_xO_y (8%)	IAA: O_x (27%)	IAA: O_xS_y (25%)	IAA: S_x (11%)
$C_{19}H_{24}$	$C_{26}H_{29}NO_2$	$C_{18}H_{14}O_2$	$C_{29}H_{50}O_3S_3$	$C_{20}H_{18}S$

Figure 1. Chemical structures of the pre-determined RA (top) and IAA (bottom) molecules. The relative abundance of each heteroatom group is shown in parentheses. Reproduced from Ballard et al., Molecular Characterization of Strongly and Weakly Interfacially Active Asphaltenes by High-Resolution Mass Spectrometry. Energy & Fuels 2020, 34 (11), 13966-13976. Copyright 2020 American Chemical Society.

Gaussian09 [40-42] was used to perform Density functional theory (DFT) calculations to optimize *in vacuo* the molecular structures of ten selected RA and IAA molecules and calculate atomic partial charges using the Merz-Singh-Kollman (MK) scheme. The detailed results are given in

Figs. S1 and S2.[40, 43-45] The optimization procedure was completed using the Becke three-parameter Lee-Yang-Parr (B3LYP) exchange-correlation functional with the 6-31G* basis set and the starting structure as exported from Avogadro.[46, 47] Successful convergence was achieved for all the molecules. B3LYP was chosen for the reliable performance over a wide range of organic molecules.[48, 49]

Intermolecular Grid-Search: Interaction structures and energies were calculated by a grid-search method, through which a probe molecule is positioned at points within a spatial grid that surrounds a target molecule.[29, 31, 35, 50-52] In the current study, an orthogonal grid of dimensions 26 Å × 26 Å × 26 Å and 9 points per axis was created such that the grid point spacing was 3.25 Å, as shown in Fig. 2. A sensitivity analysis was performed on the grid parameters. At each point on the translation grid, the probe molecule was centered and rotated as a rigid body, using a step-size in the three Euler angles, describing the orientation of 30°, 30°, 30°. The Dreiding interatomic potential was used to calculate a pairwise interaction energy at each position on the six-dimensional grid.[53] Furthermore, a low-pass filter (-0.5 kcal/mol, unless otherwise stated) was applied to remove physically unreasonable or energetically insignificant positions. The workflow applied led to an unguided, exhaustive search of the interatomic potential between the probe and target molecules. With the molecules being treated as 'rigid bodies', there is no allowance for conformational relaxation when calculating the interaction energy.
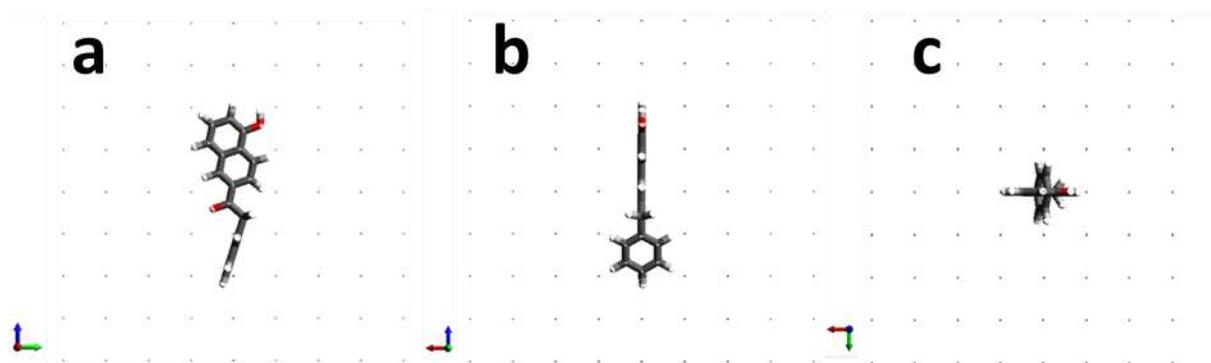

Figure 2. Grid set-up for IAA (O_x), with dimensions of 26 Å × 26 Å × 26 Å and 9 points in each axis. Oxygen atoms are shown in red. (a) Initial orientation computed according to the principal axes of the molecule; (b) rotation of the grid by 90° in the anticlockwise horizontal direction; and (c) additional rotation of 90° in the vertical direction as shown by the axis arrows in the bottom left of each image.

The Dreiding interatomic potentials were used to calculate intermolecular interactions through summation of the van der Waals (vdW), hydrogen bonding; and electrostatic interactions between the molecules constituent atoms (see Eqs. 1, 2 and 3 respectively).[53] Grid positions that result in a collision of atoms would produce a strongly positive interaction energy and were not considered. Moreover, results with an almost zero interaction energy can be removed by setting the threshold to -0.5 kcal/mol (-2.09 kJ/mol) to filter out very weak interactions due to extended molecule-molecule separation distances, and repulsive interactions that occur when two molecules overlap. The vdW is calculated as follows:

$$E_{LJ} = D^0_{j,k} \left(\left(\frac{r_{j,k}}{R^0_{j,k}} \right)^{-12} - 2 \left(\frac{r_{j,k}}{R^0_{j,k}} \right)^{-6} \right) \tag{1}$$

where E_{LJ} is the combined repulsion and dispersion potential energy (subscript LJ is the Lenard-Jones 12-6 type expression), $D^0_{j,k}$ is the energy well depth for the pairwise interaction between atom types j and k, $r_{j,k}$ is the separation distance between atoms j and k (Å), and $R^0_{j,k}$ is the equilibrium separation distance between atoms j and k. The hydrogen bonding is calculated by:

$$E_{HB} = D_{HB} \left(5 \left(\frac{R^0_{DA}}{r_{DA}} \right)^{12} - 6 \left(\frac{R^0_{DA}}{r_{DA}} \right)^6 \right) \cos^4 (\theta_{DHA}) \tag{2}$$

where E_{HB} is the hydrogen bonding potential energy based on separation distance, r_{DA} is the distance between the hydrogen bond donor acceptor atoms in (Å), D_{HB} is the potential energy well depth for a hydrogen bond (fixed at 7 kcal/mol),[53] R^0_{DA} is the equilibrium separation distance between a hydrogen bond donor and acceptor atom (2.75 Å), and θ_{DHA} is the bond angle subtended at the hydrogen atom between the donor and acceptor atoms. In Dreiding, the parameters D_{HB} and R^0_{DA} are allocated the same values irrespective of the donor and acceptor atom identity (nitrogen and oxygen). All hydrogen bonds with $\theta_{DHA} < 90°$ were not calculated, in accordance with the Dreiding force field method. The electrostatic interaction is calculated by:

$$E_Q = (322.0637)Q_j Q_k / \epsilon R_{jk} \tag{3}$$

where Q_j and Q_k are the charges in electron units of atoms j and k, R_{jk} is the separation distance between the atoms (Å), ϵ is the dielectric constant and 332.0637 converts E_Q into kcal/mol.

A sensitivity analysis on the selected grid parameters was completed which included the spacing between grid points and the Euler angles of rotation (i.e. rotational angles). The rotation angles (θ) become more important with increasing molecule size. For example, as the distance from the centre of the molecule increases (r), the spatial distance (s) between each rotation increases ($s = r\theta$). The fine-grained orthogonal grid consisted of 9 points in each axis with dimensions 20 Å × 20 Å × 20 Å and a step-size in the three Euler angles of 10°, 10°, 10°.

Data Analysis: Using the grid setup and interrogation steps, many of the calculated interaction energies were found to be very low due to the large separation distances, or positive due to overlapping molecules. Therefore, data analysis predominantly considered the top 100 favored (strongest) molecule-molecule interactions. Violin plots[54] with interaction energies between -8 and 0 kcal/mol (-33.47 and 0 kJ/mol) were created to visualize the distribution of interaction energies, with more negative values corresponding to stronger molecular interactions. The violin plots may be described as vertical histograms, with Kernel density estimation (KDE) smoothing applied.

RESULTS AND DISCUSSION

Grid Granularity and Rotation Angles: A grid sensitivity analysis was conducted to assess the influence of grid granularity and rotation angles on the interaction energies (vdW, electrostatic and hydrogen bonding) between the probe and target molecules. For analysis, the IAA model structure of O_xS_y was chosen as the probe and target molecules due to its high relative abundance in the IAA fraction and the presence of O and S which have been noted for their importance in governing the behavior of IAA.[6, 12, 13, 20, 55]

Taking the largest asphaltene molecules, the minimum grid size was determined based on twice the radius plus the separation between two grid points, giving a minimum grid size of ~20 Å. When increasing the grid size from 20 Å^3 to 26 Å^3, the spacing between the grid points increased from 2.5 Å to 3.25 Å. However, the change in interaction energies was found to be

minimal, with the mean total interaction energy, based on the top 100 most favored interactions, decreasing from -4.96 kcal/mol (-20.75 kJ/mol) for the small grid to -4.47 kcal/mol (-18.80 kJ/mol) for the large grid, a 9.4% decrease in the overall interaction energy. The contribution from electrostatic interactions was found to increase from 16.1% (small grid) to 23.1% (large grid), with the remaining contribution from vdW interaction only. While certain studies may require the use of the smallest grid to elucidate the preferred orientation of the strongest interaction, in the current study, a larger grid was of interest as it allowed multiple strong interactions to be interrogated which was of greater interest when studying the complex structures of interacting asphaltene molecules. The larger grid allowed for improved agility/rapidity of the approach without sacrificing too much the precision of the results and avoided repetition of a single interaction which can bias the data.[36] In fixing the grid size, the relative changes in total interaction energies are directly correlated to the differences in asphaltene structure and chemistry.

Figure 3 compares the coarse-grained (CG) and fine-grained (FG) models and shows the three most favored interactions as calculated by the grid search method. The parameters used for the coarse- and fine-grained models were CG – grid point spacing 26 Å × 26 Å × 26 Å, rotational angles 30°, 30°, 30°; and FG – grid point spacing 20 Å × 20 Å × 20 Å, rotational angles 10°, 10°, 10°. For the FG model, the strongest interaction energies were found to be ~30% larger than those obtained from the CG model, and demonstrate the sensitivity of the grid refinement on determining the optimal interaction between the two asphaltene molecules. The interaction energies are within the range predicted for asphaltenic material elsewhere.[22, 24] However, the top 3 interactions of the FG model were all slight refinements of the same interaction, and thus when comparing the energy contributions of the top 100 favored interactions, the energy map would be biased by the same strong interaction. While the FG model would be appropriate to determine the strongest interaction, it would not satisfy the objectives of the current study. This validates the choice to use a CG model to probe different molecular interactions rather than repeat sampling of a favored interaction. Using the FG model, the contribution from electrostatic interactions (top 100 most favored interactions) was 26.4% of the total energy, which reduced slightly to 23.1% for the CG model.
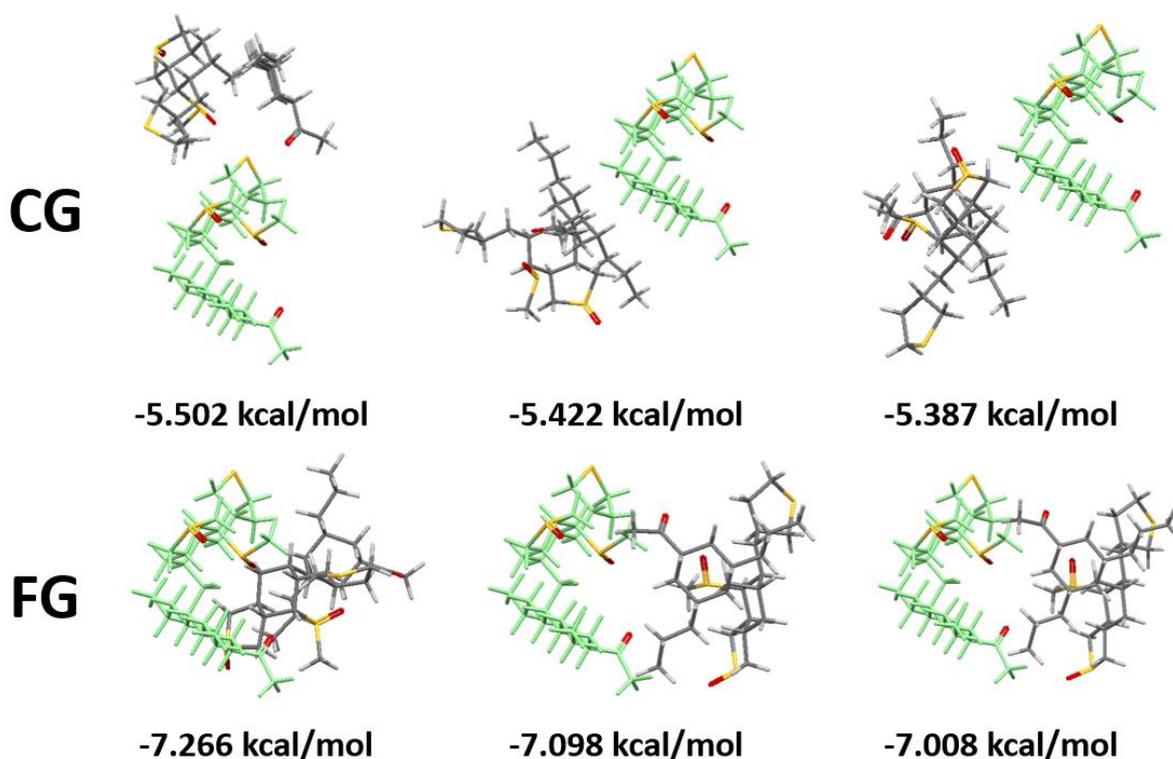
Figure 3. Grid refinement analysis showing the three most favored interactions between IAA O_xS_y for CG and FG models. With the FG model the same interaction is refined, however, for the CG model three different interactions between the two asphaltene molecules are revealed. The probe and target molecules are identified by the green and gray color shadings respectively.

IAA and RA Interaction with Water: The interaction of the different asphaltene molecules with water is particularly interesting, since the method of separating whole asphaltenes based on their interfacial activity at oil-water interfaces has led to a new understanding of the physicochemical properties of emulsion-stabilizing asphaltenes. Figure 4a shows the pairwise interaction energy distribution (top 1000 strongest interactions) for IAA O_xS_y and RA O_xS_y interacting with a water molecule. For both asphaltene molecules, and the most favored interactions, the contribution from vdW was found to be negligible with the total interaction energy dependent on hydrogen bonding and electrostatic interactions. For the weaker interactions (top 100), the total interaction energy is strongly influenced by the electrostatic interactions, and reflects the contribution from the heteroatoms, with a slightly greater contribution from oxygen due to its higher partial charge (Fig. S1 and S2). For the most favorable interactions (top 100), the electrostatic interactions remain, but the contribution from hydrogen bonding becomes more significant.

The location of the strongest interactions can be visualized by color mapping the position of the probe molecule relative to the target molecule, with the threshold minimum interaction energy identified by blue (-0.5 kcal/mol), green (-1.0 kcal/mol), yellow (-1.5 kcal/mol), orange (-2.0 kcal/mol) and red (-2.5 kcal/mol) spheres, see Fig. 4. For IAA O_xS_y, the strongest interactions are clustered around the oxygen containing groups, with both the sulfoxide and carboxylic groups interacting strongly with the hydrogen atoms of water. Compared to RA O_xS_y, the multi-core structure and multiple heteroatoms of IAA O_xS_y means that it exhibits a greater number of strong interactions at multiple locations and thus will preferentially interact with water molecules.
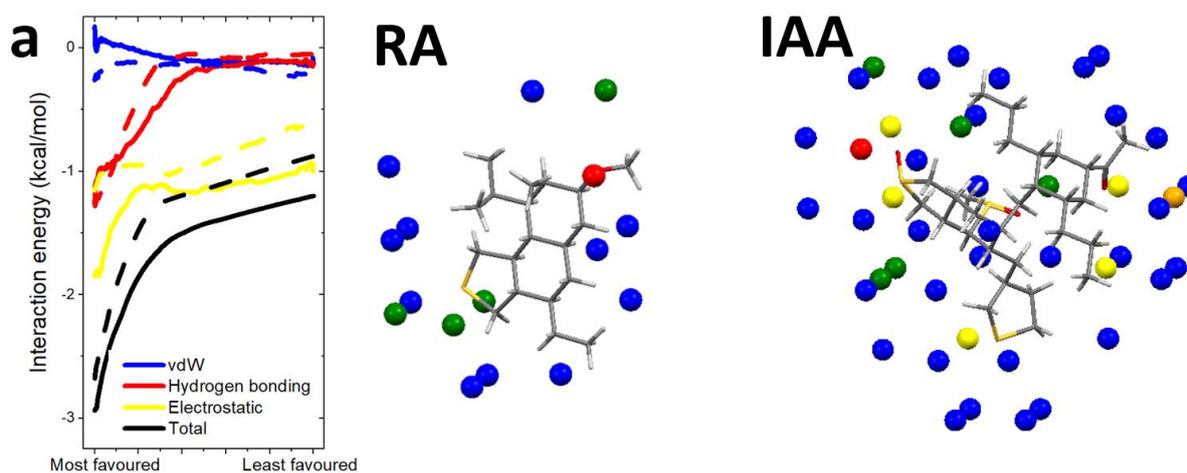

Figure 4. a) The energy contributions from vdW (blue), hydrogen bonding (red) and electrostatic (yellow) interaction are shown for the top 1000 interactions, ranked from the most favored (strongest) to least favored (weakest) interactions. Solid and dashed lines represent the IAA and RA data, respectively. Interaction energy map between a water molecule (probe) and target molecule RA O_xS_y and IAA O_xS_y. Threshold interaction energies: -0.5 kcal/mol (blue), -1.0 kcal/mol (green), -1.5 kcal/mol (yellow), -2 kcal/mol (orange), -2.5 kcal/mol (red). The most energetically favored positions are clustered ($\sim$3.0 Å) around the heteroatoms in both RA and IAA.

The data shown in the Fig. 5 inset highlight the relative contributions of the 3 interaction energy contributions for each asphaltene molecule (RA and IAA contributions shown left and right of

the center axis), which is then considered as an overall abundance-weighted interaction, see Fig. 5 (Fig. 1 provides the relative abundance of each asphaltene molecule). Considering the interactions between a single water molecule and the 10 model asphaltene structures (5 IAA and 5 RA), the abundance-weighted mean interaction energies of IAA–H_2O and RA–H_2O were calculated to be -2.22 and -1.51 kcal/mol (-9.29 and -6.32 kJ/mol), based on the top 100 interactions. This is a 47% increase in the interaction energy of IAA relative to RA, and confirms the stronger interaction of IAA with H_2O, verifying experimental studies which confirmed the preference of IAA to reside at an oil-water interface. The relative contributions of vdW, hydrogen bonding and electrostatic interaction energies were 10%, 24% and 66% for IAA–H_2O compared to 20%, 19% and 61% for RA–H_2O. For the electrostatic interactions, the strongest interactions are seen for heteroatoms with greater partial charges.[56] For example for IAA, the oxygen atoms in the O_x asphaltene molecule have a partial charge between -0.46 to -0.55 kcal/mol (-1.93 to -2.30 kJ/mol) compared to -0.42 to -0.48 kcal/mol (-1.76 to -2.01 kJ/mol) in the O_xS_y asphaltene molecule, with the higher partial charge resulting in stronger interactions with the water molecule (inset Fig. 5).
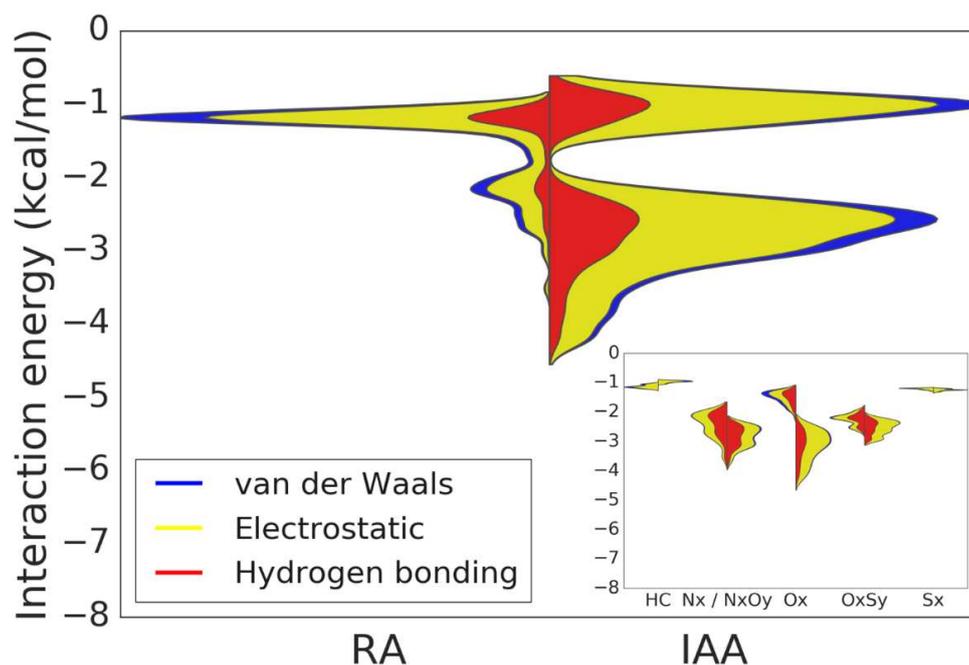
Figure 5. Violin plots showing the abundance-weighted mean interaction energies for RA (left of centre axis) and IAA (right of centre axis) interacting with a single water molecule. The interaction of the individual asphaltene molecules with water are shown inset. The contributions from vdW, electrostatic and hydrogen bonding are shown in blue, yellow and red respectively. The area of each color reflects the relative contribution to the overall interaction energy. Inset: individual asphaltene molecules interacting with a single water droplet. The asphaltene molecules were determined based on heteroatom type and are equivalent for RA and IAA except for RA N_x and IAA N_xO_y, since IAA N_x was not significantly abundant in the IAA fraction.[6]

Asphaltene-asphaltene Interactions: Using the grid-search method, interactions between RA-RA molecules and IAA-IAA molecules were studied to elucidate possible modes of interaction that will influence nanoaggregate size and shape. The 10 asphaltene molecules (5 RA and 5 IAA) are shown in Fig. 1 along with their relative abundance in each fraction. To determine the range of interaction energies and the contributions from vdW, electrostatic and hydrogen bonding to the total energy, the relative abundance of each asphaltene molecule was used to determine the likelihood of an interaction in a mixture of all asphaltene molecules. The interaction map in Fig. 6a shows all possible interactions between an asphaltene molecule and the four other asphaltene molecules in the fraction (RA or IAA). The probability of each interaction is calculated based on the relative abundance of each asphaltene group, with the

approach assuming that within a homogeneous mixture of asphaltene molecules, all interactions are statistically equal with no bias. A violin plot of the abundance-weighted mean interaction energies for the top 100 interactions of RA-RA and IAA-IAA are shown in Fig. 6b. To do this, each heteroatom group was abundance weighted to allow for differences in concentrations of the heteroatom groups in the overall asphaltene fraction.
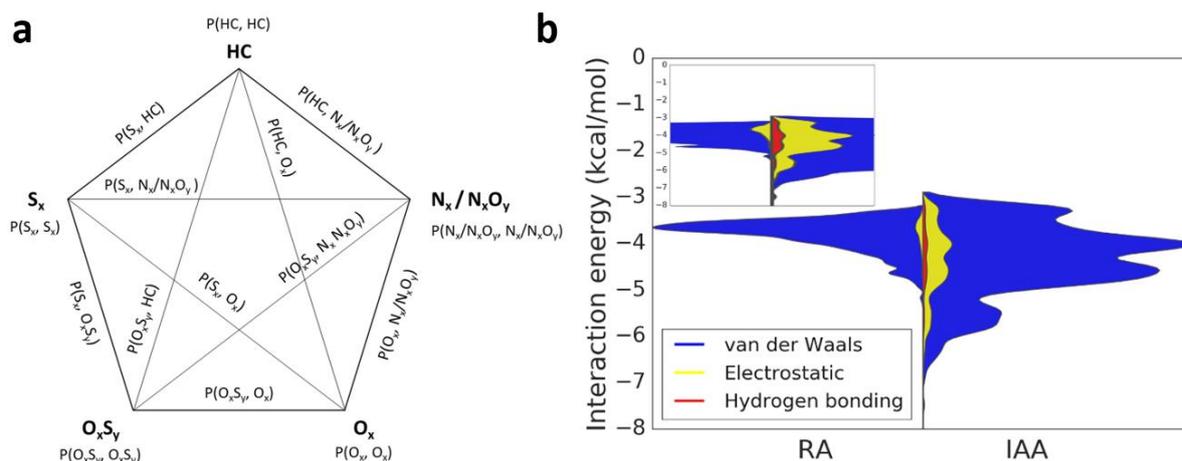

Figure 6. a) Interaction map summarizing all possible interactions (a total of 15 possible interactions) between the five asphaltene molecules in each subfraction (Fig. 1). $P(x,y)$ denotes the probability of asphaltene x interacting with asphaltene y, which is calculated based on the relative abundance of each asphaltene group. b) Violin plots showing the abundance-weighted mean interaction energies for RA-RA (left of center axis) and IAA-IAA (right of center axis). The contributions from vdW, electrostatic interactions and hydrogen bonding are shown in blue, yellow and red respectively. The area of each color reflects the relative contributions to the total interaction energy. The inset shows the same data but better highlights the contributions from electrostatic interactions and hydrogen bonding.

From the top 100 interactions, the abundance-weighted mean interaction energies of IAA-IAA and RA-RA were calculated to be -4.36 and -3.80 kcal/mol (-18.24 and -15.90 kJ/mol), and the relative contributions of vdW, hydrogen bonding and electrostatic interaction were 89%, 2% and 9% for IAA and 97%, 0% and 3% for RA. Since the grid-search method treats all molecules as rigid bodies, the difference between the overall interaction energies would likely increase were conformational freedom of structures considered. With a higher abundance of

multi-core structures, the IAA molecules would likely relax to form a more optimal dimer structure that increases the total interaction energy. However, with a prevalence of single-core motifs in the RA fraction, the contribution of molecular relaxation to a more favorable orientation would be less significant. It is important to emphasize that the grid-search method is the first-step in demonstrating a useful atomic/molecular screening approach which provides an ideal triaging tool for assessing a wide range of different molecular structures. As such it is an ideal tool that can be used to rapidly screen interactions between complex asphaltene structures and other species and should can be considered as a tool to complement the precision molecular modelling tools.

When considering the strongest interactions with energies less than -5 kcal/mol (-20.92 kJ/mol), a total of 167 possible interactions were identified, of which 97.6% were IAA-IAA interactions and 2.4% were RA-RA interactions. For IAA, 78.8% of the interaction energy was vdW, 6.1% hydrogen bonding and 15.1% electrostatic interactions, compared to 99.5% being vdW for RA. Further lowering the interaction energy threshold to -6 kcal/mol (-25.10 kJ/mol), all interactions were IAA-IAA. Comparing the relative contributions of vdW, hydrogen bonding and electrostatic interactions for these IAA-IAA interactions, the contributions from vdW, hydrogen bonding and electrostatic interactions were 64.3%, 14.3%, and 21.4%.

The dimer structures of four asphaltene fractions are shown in Fig. 7 and represent the most favorable interactions between asphaltenes in IAA (N_xO_y, O_xS_y) and RA (N_x, O_xS_y) fractions. The total interaction energies of the four asphaltene molecules are: RA N_x -6.09 kcal/mol (-25.48 kJ/mol); RA O_xS_y -4.43 kcal/mol (-18.54 kJ/mol); IAA N_xO_y -5.92 kcal/mol (-24.77 kJ/mol); and IAA O_xS_y -5.50 kcal/mol (-23.01 kJ/mol). The relative contribution of vdW energy increases in the order IAA O_xS_y < RA O_xS_y < IAA N_xO_y < RA N_x, with the reverse order determined for the relative contribution of the electrostatic interaction energy. The dimer orientation of the two asphaltene molecules differs from π-π stacking as the relative contribution of the electrostatic energy increases. For IAA O_xS_y, the electrostatic interaction accounts for 27% of the total interaction energy, with the sulfoxide groups strongly contributing to the electrostatic interactions. The grid-search method verifies that the more polar asphaltenes tend to interact via strongly electro-negative oxygen atoms, and not π-π stacking of the aromatic cores. Such findings qualitatively complement recent structural characterization of asphaltene nanoaggregates measured by SANS.[20] Studying the two

asphaltene subfractions (IAA and RA) and using a shape-independent modeling method to determine the characteristic length and Lorentzian exponents, the nanoaggregate characteristic length of IAA was more than double that of RA, with the Lorentzian exponents of 2.9 for IAA as compared to 2.2 for RA. These values confirmed that RA nanoaggregates were smaller and more compact than IAA nanoaggregates. It was hypothesized that such differences resulted from different interaction mechanisms influenced by the higher heteroatom content of IAA. Clarifying the nature of the interaction between IAA (strongly interfacially active asphaltenes) provides new insights into appropriate modes of intervention that can be exploited to disperse asphaltene molecules and prevent nanoaggregate/cluster formation. For a more quantitative comparison between modelling and experiments an approach would be to synthesize model asphaltene motifs following the methods of Wang et al.,[57] and Niu et al.[58].
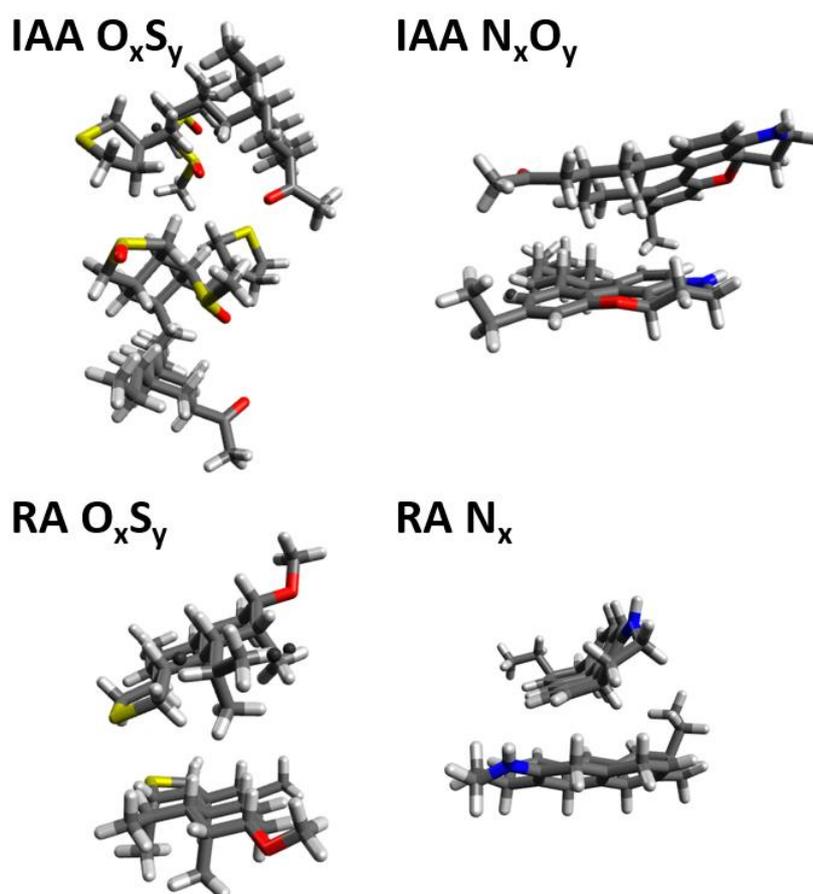

Figure 7. Most favorable interactions of IAA O_xS_y, IAA N_xO_y, RA O_xS_y and RA N_x calculated using the grid-search method. A 360° perspective of the four dimer orientations is provided in the Supplementary Information videos.

Asphaltene-solvent Interactions: The overall interaction energies of all 10 asphaltene molecules interacting with a single toluene or heptane molecule are shown in Fig. 8. These two solvent molecules were chosen as they are very typical solvents in asphaltene studies and mimic the aromatic/aliphatic components of real crude oils. For IAA and the top 100 interactions, the abundance-weighted contributions from vdW, hydrogen bonding and electrostatic interactions were 93.6%, 0% and 6.4% with toluene, and 99.7%, 0% and 0.3% with heptane. For RA and the top 100 interactions, the abundance-weighted contributions from vdW, hydrogen bonding and electrostatic interactions were 96.2%, 0% and 3.8% with toluene, and 98.1%, 0% and 1.9% with heptane. Although the vdW interaction strongly dominates behavior in both toluene and heptane, the electrostatic contribution in IAA-toluene is 6.4%, which can be attributed to the high polarity (partial charges shown in Fig. S1 and S2) of the IAA molecules interacting with the methyl group of toluene.

For the top 100 interactions of each asphaltene molecule, the abundance-weighted mean interaction energies were -3.66 kcal/mol (-15.31 kJ/mol) and -3.62 kcal/mol (-15.15 kJ/mol) for IAA-toluene and RA-toluene, and -2.98 kcal/mol (-12.47 kJ/mol) and -2.76 kcal/mol (-11.55 kJ/mol) for IAA-heptane and RA-heptane. These differences confirm stronger interaction between asphaltene-toluene than asphaltene-heptane, as would be expected based on their relative solubilities in the two solvents.
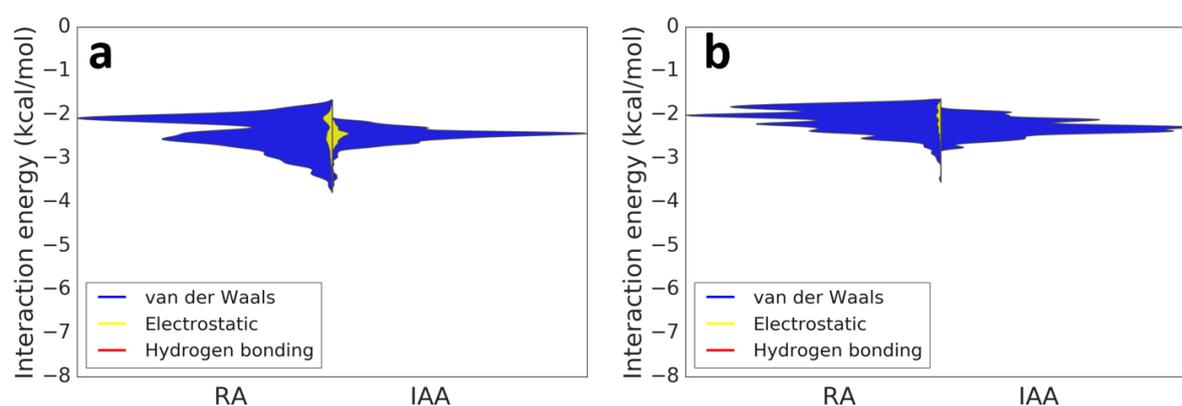

Figure 8. Violin plots showing the abundance-weighted mean interaction energies for RA (left of centre axis) and IAA (right of centre axis) interacting with a single toluene molecule (a) and a single heptane molecule (b). The contributions from vdW, electrostatic and hydrogen bonding are shown in blue, yellow and red respectively. The area of each color reflects the relative contribution to the overall interaction energy.

Although full solvation of an asphaltene molecule was not performed due to complexity in determining the critical number of solvent molecules for full solvation, a comparison of the asphaltene-solvent and asphaltene-asphaltene interaction energies can shed-light on the relative asphaltene solubility. The stability index is based on nucleation theory, where the balance of solute-solute, solute-solvent and solvent-solvent interactions govern solubility, and in the current study is taken as the ratio of asphaltene-asphaltene to asphaltene-toluene interaction energies.[59] A smaller stability index suggests greater solubility of the asphaltene molecule in toluene.

The top 100 most favored asphaltene-asphaltene and asphaltene-solvent interactions for each asphaltene molecule are compared in Table 1. While the interaction energy between asphaltene-toluene vary slightly for the different asphaltene molecules, the more significant variations in energy occur in the dimer formation of the different asphaltene molecules, especially the IAA fraction. As such, the stability index for the IAA molecules tend to be greater than those for the RA molecules, and would indicate poorer solubility of IAA relative to RA. This is in good agreement with experiments where it has been shown that IAA is less soluble than RA in toluene.[20] The grid-search method elucidates that poorer solubility is mostly associated with those asphaltenes that exhibit small multi-core structures and contain O and S heteroatoms, particularly in the form of carbonyl, hydroxyl and sulfoxide functional groups. While the output is informative, interpretation of the grid-search results are only qualitative, with the method used as a first-step in the screening of large structural databases to identify interactions of interest which can then be investigated further using more computationally intensive techniques such as MD.

Table 1. Summary of interaction energies between asphaltene-asphaltene and asphaltene-toluene. The relative solubility of each asphaltene molecule can be inferred from the stability index which is calculated as a ratio of the interaction energies. The stability index is color coded to visualize the changing relative solubility with dark green and red colors representing the most stable and least soluble asphaltene groups, respectively.

		HC	N_x / N_xO_y	O_x	O_xS_y	S_x
Interaction energy (kcal/mol)	**RA - toluene**	-3.281	-3.657	-3.468	-3.407	-2.966
	RA - itself	-4.720	-6.090	-5.041	-4.429	-5.580
	Stability index	1.439	1.665	1.454	1.300	1.881
	IAA - toluene	-2.654	-3.616	-2.787	-2.758	-2.982
	IAA - itself	-4.727	-5.920	-7.257	-5.502	-4.996
	Stability index	1.781	1.637	2.604	1.995	1.675

CONCLUSIONS

Prior research revealed differences in the physicochemical properties of strongly and weakly interfacially active asphaltenes. Characteristics of the strongly interfacially active asphaltenes include: i) increased partitioning at oil-water interfaces; ii) lower solubility in toluene; and iii) larger more porous nanoaggregates. [12-14, 20, 55] Using the grid-search method to calculate the structural nature and energetics associated with intermolecular interactions between probe molecules with target molecules, the effect of the asphaltene molecular structure on those characteristics has been further clarified.

i) The increased contributions from electrostatic interactions and hydrogen bonding account for the stronger interaction energy between IAA-H_2O than RA-H_2O, with the strong electrostatic interactions attributed to the higher partial charges of O and S atoms.

ii) With small differences in the abundance-weighted mean interaction energies of IAA-solvent molecule and RA-solvent molecule (dimer structures), the poorer solubility of IAA in toluene is partly attributed to the stronger interaction energy between two asphaltene molecules.

iii) The abundance-weighted mean interaction energy for IAA-IAA and RA-RA was -18.24 and -15.90 kJ/mol, respectively. The RA-RA interaction was almost entirely vdW interactions (97%), whereas electrostatic interactions (9%) and hydrogen bonding (2%) contributed to the overall interaction energy of IAA-IAA. The

strongest interactions below the interaction energy threshold of -25.10 kJ/mol were all IAA-IAA. With increasing contribution from electrostatic interactions, the dimer orientation less resembles $\pi - \pi$ stacking, inferring deviation from the Yen-Mullins aggregation model when asphaltenes are small, multi-core and heteroatom rich.

The study demonstrated the potential to rapidly obtain insightful and molecular-scale information about complex asphaltene-solvent and asphaltene-asphaltene interactions. Combining the grid-search method with a more comprehensive database of representative asphaltene structures, as is now possible through the growth of Petroleomics, can provide a valuable tool for screening hundreds or thousands of interactions between asphaltenes, solvent molecules and dispersant molecules. These calculations will assist in furthering our understanding to design appropriate strategies to better control behavior of asphaltenes in different chemical environments.

ASSOCIATED CONTENT

Supplementary Information

A1. Partial charges of the model structures.

A2. 360° perspective of the four dimer orientations (videos).

AUTHOR INFORMATION

Corresponding Author

*Email: D.Harbottle@leeds.ac.uk

Notes

The authors declare no competing financial interest.

REFERENCES

1.   Mullins, O. C., The Asphaltenes. *Annual Review of Analytical Chemistry* **2011,** *4* (1), 393-418.

2.   Yarranton, H. W.; Ortiz, D. P.; Barrera, D. M.; Baydak, E. N.; Barré, L.; Frot, D.; Eyssautier, J.; Zeng, H.; Xu, Z.; Dechaine, G.; Becerra, M.; Shaw, J. M.; McKenna, A. M.; Mapolelo, M. M.; Bohne, C.; Yang, Z.; Oake, J., On the Size Distribution of Self-Associated Asphaltenes. *Energy & Fuels* **2013,** *27* (9), 5083-5106.

3.   Giraldo-Dávila, D.; Chacón-Patiño, M. L.; McKenna, A. M.; Blanco-Tirado, C.; Combariza, M. Y., Correlations between Molecular Composition and Adsorption, Aggregation, and Emulsifying Behaviors of PetroPhase 2017 Asphaltenes and Their Thin-Layer Chromatography Fractions. *Energy & Fuels* **2018,** *32* (3), 2769-2780.

4.   Chacón-Patiño, M. L.; Smith, D. F.; Hendrickson, C. L.; Marshall, A. G.; Rodgers, R. P., Advances in Asphaltene Petroleomics. Part 4. Compositional Trends of Solubility Subfractions Reveal that Polyfunctional Oxygen-Containing Compounds Drive Asphaltene Chemistry. *Energy & Fuels* **2020,** *34* (3), 3013-3030.

5.   Niles, S. F.; Chacón-Patiño, M. L.; Smith, D. F.; Rodgers, R. P.; Marshall, A. G., Comprehensive Compositional and Structural Comparison of Coal and Petroleum Asphaltenes Based on Extrography Fractionation Coupled with Fourier Transform Ion Cyclotron Resonance MS and MS/MS Analysis. *Energy & Fuels* **2020,** *34* (2), 1492-1505.

6.   Ballard, D. A.; Chacón-Patiño, M. L.; Qiao, P.; Roberts, K. J.; Rae, R.; Dowding, P. J.; Xu, Z.; Harbottle, D., Molecular Characterization of Strongly and Weakly Interfacially Active Asphaltenes by High-Resolution Mass Spectrometry. *Energy & Fuels* **2020,** *34* (11), 13966-13976.

7.   Zhang, Y.; Siskin, M.; Gray, M. R.; Walters, C. C.; Rodgers, R. P., Mechanisms of Asphaltene Aggregation: Puzzles and a New Hypothesis. *Energy & Fuels* **2020,** *34* (8), 9094-9107.

8.   Mullins, O. C.; Sabbah, H.; Eyssautier, J.; Pomerantz, A. E.; Barré, L.; Andrews, A. B.; Ruiz-Morales, Y.; Mostowfi, F.; McFarlane, R.; Goual, L.; Lepkowicz, R.; Cooper, T.; Orbulescu, J.; Leblanc, R. M.; Edwards, J.; Zare, R. N., Advances in Asphaltene Science and the Yen–Mullins Model. *Energy & Fuels* **2012,** *26* (7), 3986-4003.

9.   Gray, M. R.; Tykwinski, R. R.; Stryker, J. M.; Tan, X., Supramolecular Assembly Model for Aggregation of Petroleum Asphaltenes. *Energy & Fuels* **2011,** *25* (7), 3125-3134.

10.   Gray, M. R.; Yarranton, H. W., Quantitative Modeling of Formation of Asphaltene Nanoaggregates. *Energy & Fuels* **2019,** *33* (9), 8566-8575.

11.   Bake, K. D.; Craddock, P. R.; Bolin, T. B.; Abdallah, W.; Mitra-Kirtley, S.; Andrews, A. B.; Mullins, O. C.; Pomerantz, A. E., Structure-Solubility Relationships in Coal, Petroleum, and Immature Source-Rock-Derived Asphaltenes. *Energy & Fuels* **2020,** *34* (9), 10825-10836.

12. Qiao, P.; Harbottle, D.; Tchoukov, P.; Wang, X.; Xu, Z., Asphaltene Subfractions Responsible for Stabilizing Water-in-Crude Oil Emulsions. Part 3. Effect of Solvent Aromaticity. *Energy & Fuels* **2017,** *31* (9), 9179–9187.

13. Yang, F.; Tchoukov, P.; Dettman, H.; Teklebrhan, R. B.; Liu, L.; Dabros, T.; Czarnecki, J.; Masliyah, J.; Xu, Z., Asphaltene Subfractions Responsible for Stabilizing Water-in-Crude Oil Emulsions. Part 2: Molecular Representations and Molecular Dynamics Simulations. *Energy & Fuels* **2015,** *29* (8), 4783-4794.

14. Yang, F.; Tchoukov, P.; Pensini, E.; Dabros, T.; Czarnecki, J.; Masliyah, J.; Xu, Z., Asphaltene Subfractions Responsible for Stabilizing Water-in-Crude Oil Emulsions. Part 1: Interfacial Behaviors. *Energy & Fuels* **2014,** *28* (11), 6897–6904.

15. Subramanian, S.; Simon, S.; Gao, B.; Sjöblom, J., Asphaltene fractionation based on adsorption onto calcium carbonate: Part 1. Characterization of sub-fractions and QCM-D measurements. *Colloids and Surfaces A: Physicochemical and Engineering Aspects* **2016,** *495* (Supplement C), 136-148.

16. Subramanian, S.; Sørland, G. H.; Simon, S.; Xu, Z.; Sjöblom, J., Asphaltene fractionation based on adsorption onto calcium carbonate: Part 2. Self-association and aggregation properties. *Colloids and Surfaces A: Physicochemical and Engineering Aspects* **2017,** *514*, 79-90.

17. Wu, X., Investigating the Stability Mechanism of Water-in-Diluted Bitumen Emulsions through Isolation and Characterization of the Stabilizing Materials at the Interface. *Energy & Fuels* **2003,** *17* (1), 179-190.

18. Czarnecki, J.; Tchoukov, P.; Dabros, T., Possible Role of Asphaltenes in the Stabilization of Water-in-Crude Oil Emulsions. *Energy & Fuels* **2012,** *26* (9), 5782-5786.

19. Stanford, L. A.; Rodgers, R. P.; Marshall, A. G.; Czarnecki, J.; Wu, X. A., Compositional Characterization of Bitumen/Water Emulsion Films by Negative- and Positive-Ion Electrospray Ionization and Field Desorption/Ionization Fourier Transform Ion Cyclotron Resonance Mass Spectrometry. *Energy & Fuels* **2007,** *21* (2), 963-972.

20. Ballard, D. A.; Qiao, P.; Cattoz, B.; Dowding, P. J.; Prevost, S.; Alshamsi, M.; Charpentier, T.; Roberts, K. J.; Xu, Z.; Harbottle, D., Aggregation Behavior of E-SARA Asphaltene Fractions Studied by Small-Angle Neutron Scattering. *Energy & Fuels* **2020,** *34* (6), 6894-6903.

21. Kuznicki, T.; Masliyah, J. H.; Bhattacharjee, S., Aggregation and Partitioning of Model Asphaltenes at Toluene−Water Interfaces: Molecular Dynamics Simulations. *Energy & Fuels* **2009,** *23* (10), 5027-5035.

22. Headen, T. F.; Boek, E. S.; Skipper, N. T., Evidence for Asphaltene Nanoaggregation in Toluene and Heptane from Molecular Dynamics Simulations. *Energy & Fuels* **2009,** *23* (3), 1220-1229.

23. Delgado-Buscalioni, R.; Coveney, P. V.; Riley, G. D.; Ford, R. W., Hybrid molecular-continuum fluid models: implementation within a general coupling framework. *Philosophical Transactions of the Royal Society A: Mathematical, Physical and Engineering Sciences* **2005,** *363* (1833), 1975-1985.

24. Headen, T. F.; Boek, E. S.; Jackson, G.; Totton, T. S.; Müller, E. A., Simulation of Asphaltene Aggregation through Molecular Dynamics: Insights and Limitations. *Energy & Fuels* **2017,** *31* (2), 1108-1125.

25. Rane, J. P.; Harbottle, D.; Pauchard, V.; Couzis, A.; Banerjee, S., Adsorption Kinetics of Asphaltenes at the Oil–Water Interface and Nanoaggregation in the Bulk. *Langmuir* **2012,** *28* (26), 9986-9995.

26. Pensini, E.; Harbottle, D.; Yang, F.; Tchoukov, P.; Li, Z.; Kailey, I.; Behles, J.; Masliyah, J.; Xu, Z., Demulsification Mechanism of Asphaltene-Stabilized Water-in-Oil Emulsions by a Polymeric Ethylene Oxide–Propylene Oxide Demulsifier. *Energy & Fuels* **2014,** *28* (11), 6760-6771.

27. Harbottle, D.; Chen, Q.; Moorthy, K.; Wang, L.; Xu, S.; Liu, Q.; Sjoblom, J.; Xu, Z., Problematic Stabilizing Films in Petroleum Emulsions: Shear Rheological Response of Viscoelastic Asphaltene Films and the Effect on Drop Coalescence. *Langmuir* **2014,** *30* (23), 6730-6738.

28. Drikakis, D.; Frank, M.; Tabor, G., Multiscale Computational Fluid Dynamics. *Energies* **2019,** *12*, 3272.

29. Rosbottom, I.; Pickering, J. H.; Hammond, R. B.; Roberts, K. J., A Digital Workflow Supporting the Selection of Solvents for Optimizing the Crystallizability of p-Aminobenzoic Acid. *Organic Process Research & Development* **2020,** *24* (4), 500-507.

30. Hammond, R. B.; Jones, M. J.; Roberts, K. J.; Kutzke, H.; Klapper, H., A structural study of polymorphism in phenyl salicylate: determination of the crystal structure of a meta-stable phase from X-ray powder diffraction data using a direct space systematic search method. *Zeitschrift für Kristallographie - Crystalline Materials* **2002,** *217* (9), 484-491.

31. Hammond, R. B.; Ma, C.; Roberts, K. J.; Ghi, P. Y.; Harris, R. K., Application of Systematic Search Methods to Studies of the Structures of Urea−Dihydroxy Benzene Cocrystals. *The Journal of Physical Chemistry B* **2003,** *107* (42), 11820-11826.

32. Ramachandran, V.; Murnane, D.; Hammond, R. B.; Pickering, J.; Roberts, K. J.; Soufian, M.; Forbes, B.; Jaffari, S.; Martin, G. P.; Collins, E.; Pencheva, K., Formulation Pre-screening of Inhalation Powders Using Computational Atom–Atom Systematic Search Method. *Molecular Pharmaceutics* **2015,** *12* (1), 18-33.

33. Rodríuez, J.; Sánchez-Marín, J.; Torrens, F.; Ruette, F., Molecular aggregation of polycyclic aromatic hydrocarbons. A theoretical modelling of coronene aggregation. *Journal of Molecular Structure: THEOCHEM* **1992,** *254*, 429-441.

34. Murgich, J.; Rodríguez; Aray, Y., Molecular Recognition and Molecular Mechanics of Micelles of Some Model Asphaltenes and Resins. *Energy & Fuels* **1996,** *10* (1), 68-76.

35. Hammond, R. B.; Roberts, K. J.; Smith, E. D. L.; Docherty, R., Application of a computational systematic search strategy to study polymorphism in phenazine and perylene. *Journal of Physical Chemistry B* **1999,** *103* (37), 7762-7770.

36. Hammond, R. B.; Hashim, R. S.; Ma, C.; Roberts, K. J., Grid-Based Molecular Modeling for Pharmaceutical Salt Screening: Case Example of 3,4,6,7,8,9-Hexahydro-2H-pyrimido (1,2-a) Pyrimidinium Acetate. *Journal of Pharmaceutical Sciences* **2006,** *95* (11), 2361-2372.

37. Kaiser, N. K.; Quinn, J. P.; Blakney, G. T.; Hendrickson, C. L.; Marshall, A. G., A Novel 9.4 Tesla FTICR Mass Spectrometer with Improved Sensitivity, Mass Resolution, and Mass Range. *J. Am. Soc. Mass. Spectrom.* **2011,** *22* (8), 1343-1351.

38. Beu, S. C.; Blakney, G. T.; Quinn, J. P.; Hendrickson, C. L.; Marshall, A. G., Broadband Phase Correction of FT-ICR Mass Spectra via Simultaneous Excitation and Detection. *Analytical Chemistry* **2004,** *76* (19), 5756-5761.

39. Blakney, G. T.; Hendrickson, C. L.; Marshall, A. G., Predator data station: A fast data acquisition system for advanced FT-ICR MS experiments. *Int. J. Mass spectrom.* **2011,** *306* (2), 246-252.

40. Frisch, M. J.; Trucks, G. W.; Schlegel, H. B.; Scuseria, G. E.; Robb, M. A.; Cheeseman, J. R.; Scalmani, G.; Barone, V.; Mennucci, B.; Petersson, G. A.; Nakatsuji, H.; Caricato, M.; Li, X.; Hratchian, H. P.; Izmaylov, A. F.; Bloino, J.; Zheng, G.; Sonnenberg, J. L.; Hada, M.; Ehara, M.; Toyota, K.; Fukuda, R.; Hasegawa, J.; Ishida, M.; Nakajima, T.; Honda, Y.; Kitao, O.; Nakai, H.; Vreven, T.; J. A. Montgomery, J.; Peralta, J. E.; Ogliaro, F.; Bearpark, M.; Heyd, J. J.; Brothers, E.; Kudin, K. N.; Staroverov, V. N.; Kobayashi, R.; Normand, J.; Raghavachari, K.; Rendell, A.; Burant, J. C.; Iyengar, S. S.; Tomasi, J.; Cossi, M.; Rega, N.; Millam, J. M.; Klene, M.; Knox, J. E.; Cross, J. B.; Bakken, V.; Adamo, C.; Jaramillo, J.; Gomperts, R.; Stratmann, R. E.; Yazyev, O.; Austin, A. J.; Cammi, R.; Pomelli, C.; Ochterski, J. W.; Martin, R. L.; Morokuma, K.; Zakrzewski, V. G.; Voth, G. A.; Salvador, P.; Dannenberg, J. J.; Dapprich, S.; Daniels, A. D.; Farkas, Ö.; Foresman, J. B.; Ortiz, J. V.; Cioslowski, J.; Fox, D. J. *Gaussian 09*, Gaussian, Inc.: Wallingford, CT, 2016.

41. Becke, A. D., A new mixing of Hartree–Fock and local density-functional theories. *The Journal of Chemical Physics* **1993,** *98* (2), 1372-1377.

42. Lee, C.; Yang, W.; Parr, R. G., Development of the Colle-Salvetti correlation-energy formula into a functional of the electron density. *Physical Review B* **1988,** *37* (2), 785-789.

43. Besler, B. H.; Merz Jr, K. M.; Kollman, P. A., Atomic charges derived from semiempirical methods. *Journal of Computational Chemistry* **1990,** *11* (4), 431-439.

44. Sigfridsson, E.; Ryde, U., Comparison of methods for deriving atomic charges from the electrostatic potential and moments. *Journal of Computational Chemistry* **1998,** *19* (4), 377-395.

45. Jacquemin, D.; Bahers, T. L.; Adamo, C.; Ciofini, I., What is the "best" atomic charge model to describe through-space charge-transfer excitations? *Physical Chemistry Chemical Physics* **2012,** *14* (16), 5383-5388.

46. *Avogadro: an open-source molecular builder and visualization tool*, 1.2.0; 2018.

47. Hanwell, M. D.; Curtis, D. E.; Lonie, D. C.; Vandermeersch, T.; Zurek, E.; Hutchison, G. R., Avogadro: An advanced semantic chemical editor, visualization, and analysis platform. *Journal of Cheminformatics* **2012,** *4* (17).

48.   Curtiss, L. A.; Raghavachari, K.; Redfern, P. C.; Pople, J. A., Investigation of the use of B3LYP zero-point energies and geometries in the calculation of enthalpies of formation. *Chemical Physics Letters* **1997,** *270* (5), 419-426.

49.   Tirado-Rives, J.; Jorgensen, W. L., Performance of B3LYP Density Functional Methods for a Large Set of Organic Molecules. *Journal of Chemical Theory and Computation* **2008,** *4* (2), 297-306.

50.   Rosbottom, I.; Roberts, K. J.; Docherty, R., The solid state, surface and morphological properties of p-aminobenzoic acid in terms of the strength and directionality of its intermolecular synthons. *CrystEngComm* **2015,** *17* (30), 5768-5788.

51.   Rosbottom, I.; Ma, C. Y.; Turner, T. D.; O'Connell, R. A.; Loughrey, J.; Sadiq, G.; Davey, R. J.; Roberts, K. J., Influence of Solvent Composition on the Crystal Morphology and Structure of p-Aminobenzoic Acid Crystallized from Mixed Ethanol and Nitromethane Solutions. *Crystal Growth & Design* **2017,** *17* (8), 4151-4161.

52.   Nguyen, T. T. H.; Rosbottom, I.; Marziano, I.; Hammond, R. B.; Roberts, K. J., Crystal Morphology and Interfacial Stability of RS-Ibuprofen in Relation to Its Molecular and Synthonic Structure. *Crystal Growth & Design* **2017,** *17* (6), 3088-3099.

53.   Mayo, S. L.; Olafson, B. D.; Goddard, W. A., DREIDING: a generic force field for molecular simulations. *The Journal of Physical Chemistry* **1990,** *94* (26), 8897-8909.

54.   Waskom, M. *seaborn.violinplot*, 0.10.0; GitHub: 2020.

55.   Qiao, P.; Harbottle, D.; Li, Z.; Tang, Y.; Xu, Z., Interactions of Asphaltene Subfractions in Organic Media of Varying Aromaticity. *Energy & Fuels* **2018,** *32* (10), 10478-10485.

56.   Ensing, B.; Tiwari, A.; Tros, M.; Hunger, J.; Domingos, S. R.; Pérez, C.; Smits, G.; Bonn, M.; Bonn, D.; Woutersen, S., On the origin of the extremely different solubilities of polyethers in water. *Nature Communications* **2019,** *10* (1), 2893.

57.   Wang, J.; van der Tuuk Opedal, N.; Lu, Q.; Xu, Z.; Zeng, H.; Sjöblom, J., Probing Molecular Interactions of an Asphaltene Model Compound in Organic Solvents Using a Surface Forces Apparatus (SFA). *Energy & Fuels* **2012,** *26* (5), 2591-2599.

58.   Niu, Z.; Ma, X.; Manica, R.; Yue, T., Molecular Destabilization Mechanism of Asphaltene Model Compound C5Pe Interfacial Film by EO-PO Copolymer: Experiments and MD Simulation. *The Journal of Physical Chemistry C* **2019,** *123* (16), 10501-10508.

59.   Ruckenstein, E.; Berim, G. O., Effect of solute–solute and solute–solvent interactions on the kinetics of nucleation in liquids. *Journal of colloid and interface science* **2010,** *342* (2), 528-532.